

Electron correlation effects and two-photon absorption in diamond-shaped graphene quantum dots

Tista Basak

*Mukesh Patel School of Technology Management and Engineering,
NMIMS University, Mumbai 400056, India**

Tushima Basak

Department of Physics, Mithibai College, Mumbai 400056, India[†]

Alok Shukla

*Department of Physics, School of Engineering and Applied Sciences,
Bennett University, Plot No. 8--11, TechZone II,
Greater Noida 201310, Uttar Pradesh, India and
Permanent Address: Department of Physics,
Indian Institute of Technology Bombay, Powai, Mumbai 400076, India[‡]*

Abstract

In quasi-1D π -conjugated polymers such as *trans*-polyacetylene and polyenes, electron correlation effects determine the “reversed” excited state ordering in which the lowest two-photon $2A_g$ state lies below the lowest one-photon $1B_u$ state. In this work, we present conclusive theoretical evidence of reversed excited state ordering in fairly 2D π -conjugated systems, namely, diamond-shaped graphene quantum dots (DQDs). Our electron correlated calculations show that DQDs begin to exhibit reversed excited ordering with increasing size, in disagreement with independent-particle picture. This signals the onset of strong correlation effects which renders them nonluminescent. Further, we calculate and analyze the two-photon absorption (TPA) spectra as well as photoinduced absorption (PA) spectra of these systems and find excellent agreement with the available experimental results. Our investigations demonstrate that unlike a strictly 1D system like *trans*-polyacetylene, the non-linear and excited state absorptions in DQDs are highly intricate, with several even parity states responsible for strong absorptions. Our results could play an important role in the design of graphene-based non-linear optical devices.

I. INTRODUCTION

The intricate role played by electron correlations in describing the photophysics of carbon-based systems exhibiting sp^2 hybridization has been an active area of research^{1,2}. The extensive focus of earlier experimental^{3,4} and theoretical studies⁵⁻⁸ was to determine the influence of electron correlations on one-photon allowed optical states. However, as per electric dipole selection rules in centrosymmetric systems, the optical states accessible by one-photon excitations are distinct from those obtained by two-photon excitations. Existing literature have provided exclusive evidence of the fact that one-photon allowed optical states are chiefly due to excitations comprising of one electron and one hole, while two-electron two-hole excitations can have a major contribution in the description of two-photon states⁹⁻¹¹. This signifies that the influence of electron correlation effects is more complicated in two-photon allowed states, as compared to the one-photon allowed optical states. Earlier studies on quasi-1D π -electron material *trans*-polyacetylene, and its oligomers, polyenes, have shown that the inclusion of electron correlation effects is responsible for the occurrence of the lowest energy two-photon $2A_g$ state below the lowest energy one-photon $1B_u$ state, in contrast to that expected within the one-electron Hückel and mean-field Hartree-Fock theories^{11,12}. However, such “reversed” excited state ordering as well as significant contribution of two-electron two-hole excitations in the description of two-photon states is not expected in fairly 2D and 3D systems, as the strength of electron correlations decreases with increase in the dimension of the system considered.

The study of non-linear optical properties of graphene and its fragments, in its own right, forms an extremely important field of research, with a fairly large number of experimental,¹³⁻²⁴ and theoretical²⁵⁻³² studies dedicated to the subject. An earlier study by our group on polyaromatic hydrocarbons revealed that the strength of electron correlations becomes dominant as the symmetry of molecules decreases from D_{6h} to D_{2h} point group.³³ This has motivated us to consider graphene quantum dots possessing D_{2h} point group. Our previous investigation on fairly 2D systems, namely diamond-shaped graphene quantum dots (DQDs), demonstrated that electron correlations are important in determining their linear optical properties.⁷ In addition, an earlier study from Kaxiras and co-workers,³⁴ and from our own group,³⁵ predicted that suitably aligned external electric field can induce energy-level shifts of spin-ordered edge states, giving rise to phase transition between the

well-defined magnetic states of DQDs. Given the profound influence of an external electric-field on the electronic, magnetic, and linear optical properties of DQDs, it is but natural to explore the nonlinear response of DQDs to incident optical radiation. This has motivated us not just to compute the nonlinear optical spectra of these structures, but also to explore the influence of electron correlations on them, which, to the best of our knowledge has not been done till date.

In this work, we report a computational study of two-photon absorption spectra of DQDs, which provides exclusive evidence of strong electron correlations resulting in the aforesaid reversed excited state ordering. Like polyenes, DQDs are also centro-symmetric systems, but with a higher point group symmetry D_{2h} . Thus, its even parity states belonging to irreducible representations (irreps) A_g and B_{1g} are invisible in linear spectroscopy, which can only detect its odd-parity excited states belonging to irreps B_{2u} and B_{3u} ⁷. In order to obtain a better understanding of the even parity states, and non-linear optical response of DQDs, we compute their two-photon absorption (TPA), and photoinduced absorption (PA) spectra, at the independent-particle (tight-binding), and configuration interaction (CI) levels. The CI results demonstrate that the DQDs exhibit reversed excited state ordering like polyenes, with increasing size, in complete disagreement with the independent-particle predictions. This highlights the presence of strong electron correlations in the DQDs. For the case of DQD-16 (DQD consisting of 16 carbon atoms), we compare its calculated TPA and PA spectra with the experiments for its hydrogen passivated analog pyrene³⁶, and obtain excellent agreement. We also calculate and analyze the TPA and PA spectra of DQD-30 (DQD consisting of 30 carbon atoms), and PA spectrum of DQD-48 (DQD consisting of 48 carbon atoms), for which, at present, no experimental or theoretical results exist. Our studies reveal that, due to structural anisotropy, the nonlinear optical response of DQDs is much more complicated as compared to that of 1D systems. A further extension of this work will be to analyze the implication of electron correlation effects in extended 2D carbon-based system in the thermodynamic limit, i.e., graphene. According to the Hückel tight-binding π -electron theory, 2D graphene is a semimetal. However, several studies³⁷ have proposed that the inclusion of electron-electron interactions is responsible for considerable modification of graphene's linear spectrum leading to an opening of energy gap, in contrast to the results obtained from the single-particle theory.

The organization of the rest of this paper is as follows. A brief description of the com-

putational methodology is presented in Sect. II, followed by results and discussion in Sect. III. Finally, the conclusions are given in Sect. IV.

II. COMPUTATIONAL METHODOLOGY

The geometric configurations of different DQDs considered in this work are given in fig.1. The DQDs are assumed to lie in the xy plane, with the y -axis along the longer diagonal, and the x -axis along the shorter one. We have chosen uniform carbon-carbon bond lengths of 1.40 Å, and bond angles of 120°, so that each DQD has D_{2h} symmetry. The symmetries of the relevant one-photon and two-photon excited states are B_{2u} , B_{3u} and A_g , B_{1g} , respectively, as predicted by the electric-dipole selection rules.

For performing computations, we employed Pariser-Parr-Pople (PPP) model Hamiltonian^{38,39}

$$H = -\sum_{\langle i,j \rangle, \sigma} t_0 \left(c_{i\sigma}^\dagger c_{j\sigma} + c_{j\sigma}^\dagger c_{i\sigma} \right) + U \sum_i n_{i\uparrow} n_{i\downarrow} + \sum_{i < j} V_{ij} (n_i - 1)(n_j - 1), \quad (1)$$

where $c_{i\sigma}^\dagger$ ($c_{i\sigma}$) creates (annihilates) an electron of spin σ , in the p_z orbital located on the i -th carbon atom, while $n_i = \sum_\sigma c_{i\sigma}^\dagger c_{i\sigma}$ denotes the total number of electrons on the atom. The first term in Eq. 1 denotes the hopping between i -th and j -th atoms which are nearest neighbors, with $t_0 = 2.4$ eV, for the nearest neighbor distance 1.40 Å. The second and the third terms in Eq. 1 represent the electron repulsion, with parameters U , and V_{ij} , denoting the on-site, and the long-range Coulomb interactions, respectively. The distance-dependence of V_{ij} is assumed as per Ohno relationship⁴⁰, modified to include the screening effects⁴¹

$$V_{ij} = U / \kappa_{i,j} (1 + 0.6117 R_{i,j}^2)^{1/2}, \quad (2)$$

where $\kappa_{i,j}$ is the dielectric constant of the system, included to take into account the screening effects, and $R_{i,j}$ is the distance (in Å) between the i th and j th carbon atoms. In the present set of calculations we have used the “screened parameters” of Chandross and Mazumdar⁴¹ with $U = 8.0$ eV, $\kappa_{i,j} = 2.0$ ($i \neq j$), and $\kappa_{i,i} = 1.0$. We have used these Coulomb parameters, coupled with the hopping value $t_0 = 2.4$ eV, extensively in the past for conjugated polymers^{6,42–47}, polyaromatic hydrocarbons^{33,48}, and graphene quantum dots^{7,35}. In case of a charge-neutral DQD consisting of N carbon atoms (DQD- N , with N always even),

each carbon atom contributes one π electron, and the p_z orbital of each of the carbon atom is part of the basis set. Thus, for each DQD- N treated within the PPP model, we have N basis functions, and N electrons, making it a half-filled system. Our calculations are initiated at the restricted Hartree-Fock (RHF) level using a code developed in our group⁴⁹. The mean-field approximation at the RHF level results in $N/2$ doubly-occupied orbitals filled in accordance with the aufbau principle, and $N/2$ unoccupied molecular orbitals (MOs). Pictorial representations of few of the frontier molecular orbitals contributing significantly to the non-linear properties for DQD-16, DQD-30 and DQD-48 and the Hartree-Fock wavefunction are given in Figs. S1–S4 of the Supporting Information⁵⁰. Thereafter, the PPP Hamiltonian is transformed from the site representation to the MO representation, and used to perform configuration interaction (CI) calculations to include electron-correlation effects. The electron-correlations at the CI level are incorporated by considering virtual excitations from the occupied to unoccupied orbitals (see Fig. S5 of Supporting Information⁵⁰, for a pictorial representation), leading to configuration mixing. The CI calculations are performed at the quadruple configuration interaction (QCI), or the multi-reference singles-doubles configuration interaction (MRSDCI), level depending on the size of the system. The QCI method was employed for the A_g and the B_{2u} states of DQD-16, while the MRSDCI approach was adopted for the B_{3u} and the B_{1g} symmetries of DQD-16. Further, the MRSDCI methodology was considered for optimizing all the symmetries of the larger systems DQD-30 and -48. The increase in the number of molecular orbitals, with increase in the size of DQD, leads to an enormous increase in the dimension of the CI matrix. Hence, the frozen orbital approximation was implemented for DQD-48, in order to make the computations feasible. According to this approximation, the lowest two occupied orbitals were frozen and highest two virtual orbitals were deleted so as to retain the particle-hole symmetry⁷. The many-particle wave functions thus obtained are used to compute the transition electric dipole moments between various states, which in turn are employed to calculate their TPA or PA spectra. In particular, the TPA spectrum is computed as the imaginary part of the third-order non-linear susceptibility $\chi_{ijkl}^{(3)}(\omega, \omega, \omega, -\omega)$ (i, j, k , and l denote Cartesian directions) using the sum-over-states (SOS) formula of Orr and Ward⁵¹. Henceforth, we adopt the shorthand notation $TPA_{ijkl} = \text{Im}(\chi_{ijkl}^{(3)}(\omega, \omega, \omega, -\omega))$, and in this work we present results on TPA_{xxxx} , TPA_{yyyy} , and TPA_{xyxy} , for DQD-16, and DQD-30. This PPP-CI computational methodology has been extensively utilized in our earlier works on optical properties

of π -conjugated systems^{6,7,42–47}, including their TPA spectra^{33,52}.

The states with A_g symmetry give rise to two-photon resonances in the TPA_{xxxx} and TPA_{yyyy} spectra for these DQDs. Similarly, the two-photon resonances in the TPA_{xyxy} spectrum corresponds to states having B_{1g} symmetry. In addition, the PA spectrum with respect to the first optically excited $1B_{2u}$ state has been computed for DQD-48, for which CI level TPA calculations were too time consuming. The PA spectrum for DQD-16 and DQD-30 has also been computed. It is observed that the salient features of the non-linear optical properties obtained from the PA spectrum for DQD-16 and DQD-30 are qualitatively in excellent agreement with those derived from their TPA spectra, validating our approach for the prediction of the non-linear characteristics of DQD-48 from its PA spectrum.

III. RESULTS AND DISCUSSION

In this section, we discuss the excited state ordering in the DQDs, and compare it with that observed in the polyenes. Furthermore, striking characteristics of PA, as well as TPA, spectra for the DQDs of different sizes are analyzed based upon the Hückel (tight-binding), and the CI level calculations.

A. *Excited State Ordering*

For comparison with polyenes, we will refer to the one/two-photon states of DQDs generically as B_u / A_g - type states. For accurate determination of excited state ordering in DQDs, large-scale CI calculations were performed for the first two lowest energy two-photon states ($1A_g$ ground state and $2A_g$), and first one-photon ($1B_u$) state. The dimensions of CI matrices considered for the computation of excited state ordering are given in the table S1 of the Supporting Information⁵⁰.

Table I presents the computed excitation energies of the $2A_g$ and $1B_u$ states of DQD-16, DQD-30 and DQD-48, respectively, at the Hückel (tight-binding), and CI levels. The computed energies of the $2A_g$ and $1B_u$ states at the full configuration interaction (FCI) level of 1-D n -polyene ($n = 4, 6$ and 8 carbon atoms equal to the number of carbon atoms along the longer diagonal of DQD-16, DQD-30 and DQD-48, respectively) are also given in table I, for a qualitative comparison of the nature of excited state ordering between 1-D and 2-D

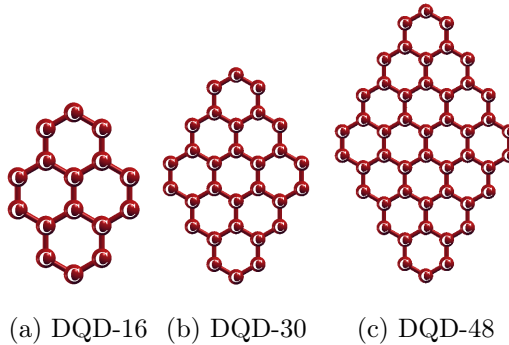


Figure 1: Geometric configuration of DQDs considered in this work: (a) DQD-16 (b) DQD-30 (c) DQD-48.

systems. In addition, theoretical values of the energies of $1B_u$ state obtained by the hybrid Hartree-Fock/density functional theory B3LYP method by Yumura *et al.*⁵³ are also reported for comparison with our results. Figure 2 represents the energies of $1B_u$ and $2A_g$ states of DQD-16, DQD-30 and DQD-48, respectively, at the Hückel and CI level.

The computed CI energies of $1B_u$ state of DQD-16 and DQD-30 at 3.60 eV and 2.45 eV, respectively, are in excellent agreement with the earlier experimental values of 3.69 eV⁵⁴ and 2.55 eV⁵⁵ for pyrene and dibenzo[bc,kl]coronene (hydrogen passivated counterpart of DQD-30), respectively, marking the high precision of our calculated results. The accuracy of the results obtained by the B3LYP method⁵³ is more than that obtained at the Hückel level, but less than those obtained at the CI level. Because of the alternant nature of the systems considered (DQDs and polyenes), Hückel model always predicts $1B_u$ state to be below $2A_g$. However, it is observed that in case of 1-D polyenes, PPP-CI calculations correctly capture the expected reversed excited state ordering with the $2A_g$ state below $1B_u$. By contrast, the PPP-CI calculations for DQD-16 predict that the $2A_g$ state lies very slightly above the $1B_u$ state, while for DQD-30 it is almost degenerate with the $1B_u$ state. However, for DQD-48, the $2A_g$ state is lowered significantly below the $1B_u$ state. Thus, we note that, at the CI level, reversed excited state ordering is realized, with increasing size of DQDs, in complete contradiction with the Hückel model results. Furthermore, the wave function of the $2A_g$ states of DQD-16, DQD-30 and DQD-48, are dominated by the double excitation $|H \rightarrow L; H \rightarrow L\rangle$, where H and L represent the highest occupied molecular orbital (HOMO), and the lowest unoccupied molecular orbital (LUMO), respectively. Both these facts clearly

DQD	$1B_u$ state (eV)	$2A_g$ state (eV)
	Hückel/B3LYP Theory ⁵³ (Ref. ⁵³)	Hückel
DQD-16	2.14/ \sim 3.8	4.06
DQD-30	0.89/ \sim 2.1	1.78
DQD-48	0.34/ \sim 1.1	0.68
	$1B_u$ state (eV)	$2A_g$ state (eV)
	PPP-CI	PPP-CI
DQD-16	3.60	3.68
DQD-30	2.45	2.44
DQD-48	1.96	1.71
4-polyene	6.08	4.83
6-polyene	5.02	3.90
8-polyene	4.43	3.32

Table I: Computed energies of $1B_u$ and $2A_g$ states of DQD-16, DQD-30 and DQD-48, respectively, at the Hückel and the CI levels. The computed energies of these states for 4-polyene, 6-polyene and 8-polyene are also given at the CI level. Theoretical values of the energies of $1B_u$ state obtained by Yumura *et al.*,⁵³ using the density functional theory (B3LYP approach), are also reported for comparison.

indicate the presence of strong electron correlations in DQDs.

A plausible qualitative explanation of the lowering of $2A_g$ state below $1B_u$, with increasing size of DQDs is as follows. DQD-16 has a 2D character with almost equal size in x and y directions resulting in relatively weaker correlation effects, rendering $1B_u$ below $2A_g$. But with increasing size, DQDs approach a more 1D character with their size along the y direction becoming larger compared to x direction, leading to stronger correlation effects, and hence, a polyene like excited state ordering with the $2A_g$ state below $1B_u$.

B. *Nonlinear Optical Properties*

In this section, we discuss the computed PA and TPA spectra of DQDs. As per SOS formulas for PA and TPA spectra,⁵¹ the widths of the intense peaks are dependent on the line-

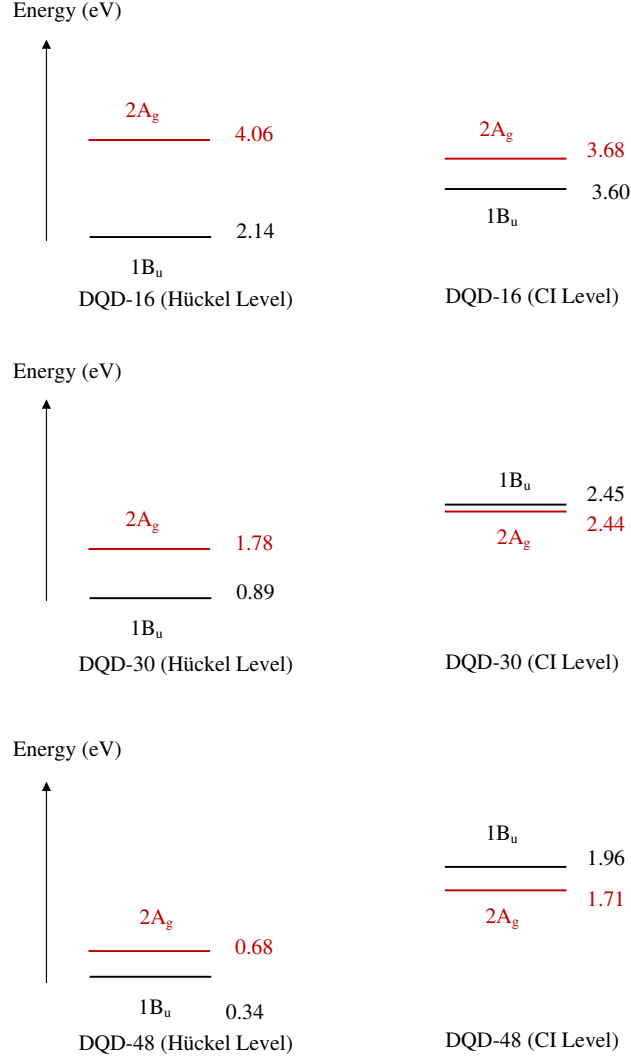


Figure 2: Schematic diagram representing the energies of $1B_u$ and $2A_g$ states of DQD-16, DQD-30 and DQD-48, respectively, at the Hückel and the CI levels.

widths of various states, which in turn depend upon carrier-lifetime, temperature, impurities etc. The heights of different peaks, on the other hand, are determined by the strengths of transition dipole operator between various states of the system, as well as the magnitude of the energy difference term in the denominator close to resonance. For computing the

photoinduced absorption and two-photon absorption spectra, the maximum energy limit of the excited states was restricted to 10 eV for CI calculations. The dimensions of CI matrices of A_g , B_{1g} , B_{2u} and B_{3u} symmetries considered for the computation of TPA and PA spectra of DQD-16, DQD-30 and DQD-48 are given in the table S2 of the Supporting Information⁵⁰.

For the purpose of validating our CI (MRSDCI and QCI) approach, we compare the calculated energies of even parity states giving rise to peaks in the computed TPA and PA spectra of DQD-16, with the earlier experimental results of its hydrogen-saturated counterpart pyrene³⁶ in Table II. The dominant wave-functions of the excited states contributing to these peaks are also given in the table. It is observed that our computed energies of the two-photon peaks of DQD-16 are in excellent quantitative agreement with the experimental data for pyrene for a number of two-photon states. The A_g peaks contributing to the TPA_{xxxx} component are not observed in the experiment, as their intensities are much less as compared to the TPA_{yyyy} component. The computed A_g state with energy 6.98 eV, giving rise to a two-photon peak at 3.49 eV, is the most intense peak in the TPA_{yyyy} spectrum (fig. 6). Wave function of this state is dominated by double excitations $|H-1 \rightarrow L; H-1 \rightarrow L\rangle + c.c.$ where the abbreviation “c.c.” represents coefficient of charge conjugate of a given singly excited configuration while the sign $(+/-)$ preceding “c.c.” implies that the two coefficients have (same/opposite) signs. This state is also responsible for the second most intense peak (IX_y) in the computed PA spectrum (fig. 4). The computed A_g state with energy 9.04 eV gives rise to an intense peak in the PA spectrum. However, it does not contribute to the TPA spectrum. Hence, the energetic ordering as well as symmetry assignment of our computed peaks are in perfect agreement with the experimental data, demonstrating the extremely high precision of our correlated electron approach. Thus, it lends credibility to our TPA/PA calculations on DQD-30 and DQD-48, for which we could not find any experimental data. In addition, it is observed that both the TPA and PA spectroscopies are efficient methods for detecting the two-photon states of this system.

1. Photoinduced Absorption

The schematic diagram describing the concept of photoinduced absorption (PA) is shown in Fig. 3. The system initially absorbs y -polarized photons from a pump laser, and gets excited from the 1^1A_g ground state to the first excited 1^1B_{2u} state. Thereafter, from a probe

Peak	CI Results/ Experiment ³⁶ (eV)	Dominant Configurations
A_g	6.98/6.93	$ H - 1 \rightarrow L; H - 1 \rightarrow L\rangle + c.c. (0.3367)$ $ H \rightarrow L; H - 1 \rightarrow L + 1\rangle (0.2960)$
B_{1g}	8.30/8.23	$ H - 6 \rightarrow L + 3\rangle + c.c. (0.2486)$ $ H - 7 \rightarrow L\rangle + c.c. (0.1678)$
B_{1g}	8.54/8.57	$ H \rightarrow L + 2; H - 3 \rightarrow L\rangle c.c. (0.2619)$ $ H - 4 \rightarrow L; H - 1 \rightarrow L + 2\rangle c.c. (0.2559)$
A_g	9.04/9.08	$ H - 3 \rightarrow L + 4; H \rightarrow L + 1\rangle - c.c. (0.2192)$ $ H - 5 \rightarrow L; H \rightarrow L\rangle + c.c. (0.1885)$
A_g	9.26/9.22	$ H \rightarrow L; H - 4 \rightarrow L + 2\rangle - c.c. (0.2015)$ $ H - 1 \rightarrow L + 1; H - 1 \rightarrow L + 1\rangle (0.1639)$

Table II: Comparison of the calculated excitation energies (in eV) of the even-parity excited states of DQD-16, contributing to peaks in its TPA and PA spectra, with the experimental data for pyrene³⁶. Note that the two-photon resonances in the absorption spectra are located at half the excitation energies. The calculations were performed at the CI level (see text for details), and the dominant configurations contributing to the many-particle wave functions of these states are also presented.

laser, it absorbs another photon polarized either in x or y directions to make a transition from the 1^1B_{2u} state to higher energy m^1B_{1g} or k^1A_g excited states, respectively. The spectrum corresponding to the probe absorption is measured, and is called the PA spectrum. Thus, the peak locations in PA spectrum correspond to the excitation energies of the even-parity states, measured with respect to the 1^1B_{2u} state. Hence, using oriented samples of DQDs, one can determine the symmetries of these even parity states, based upon the polarization of the absorbed probe photons.

In Fig. 4, we present the computed PA spectrum with respect to the first optically excited $1B_{2u}$ state for DQD-16, DQD-30 and DQD-48, respectively. Detailed quantitative information about various excited states contributing to their PA spectra is presented in the tables S9-S11 of the Supporting Information⁵⁰. Next, we summarize the important

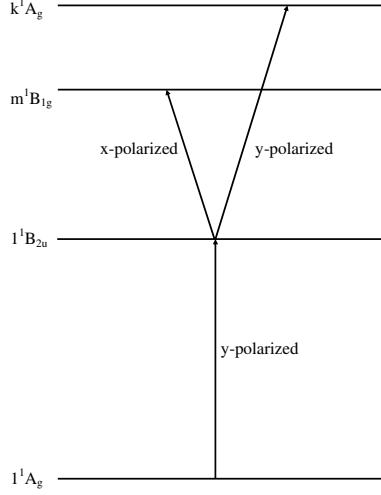


Figure 3: Schematic diagram describing the process of photoinduced absorption, along with the states involved in it. An arrow between two states denotes optical transition, with the polarization direction of the absorbed photon indicated next to it.

features of the PA spectra of the DQDs, computed at the CI level: (i) with the increasing size of the DQDs, the PA spectrum gets red-shifted, (ii) the $2A_g$ state is not observed in the PA spectra of DQD-16, DQD-30 and DQD-48 due to its weak dipole coupling to the $1B_{2u}$ state, and also because of its proximity to it, (iii) there are several high intensity peaks contributing to the PA spectra. For DQD-16, peaks $III_{x\&y}$, VII_y , $VIII_x$, IX_y and X_x make intense contribution to its PA spectrum. Of these, the most intense peak is $III_{x\&y}$ which corresponds to almost degenerate higher energy even parity states, $4A_g$ and $4B_{1g}$, having excitation energies 5.06 and 5.07 eV, respectively. The double excitation $|H \rightarrow L; H \rightarrow L\rangle$, and the single excitations $|H - 1 \rightarrow L + 3\rangle - c.c$ make dominant contributions to the many-body wave functions of these states. In case of DQD-30, the peaks III_y , IV_y , V_y and $VIII_{x\&y}$ are quite intense, with the V_y peak carrying the maximum intensity. This peak corresponds to the $10A_g$ state, with the excitation energy 4.81 eV, and the double excitation $|H - 1 \rightarrow L + 1; H \rightarrow L\rangle$ contributing mainly to its wave function. Similarly, for DQD-48, there are several peaks, namely, II_y , III_y , VII_y , and $VIII_y$ with strong intensity. Of these, the most intense peak is VII_y , corresponding to the $16A_g$ state with excitation energy 4.19

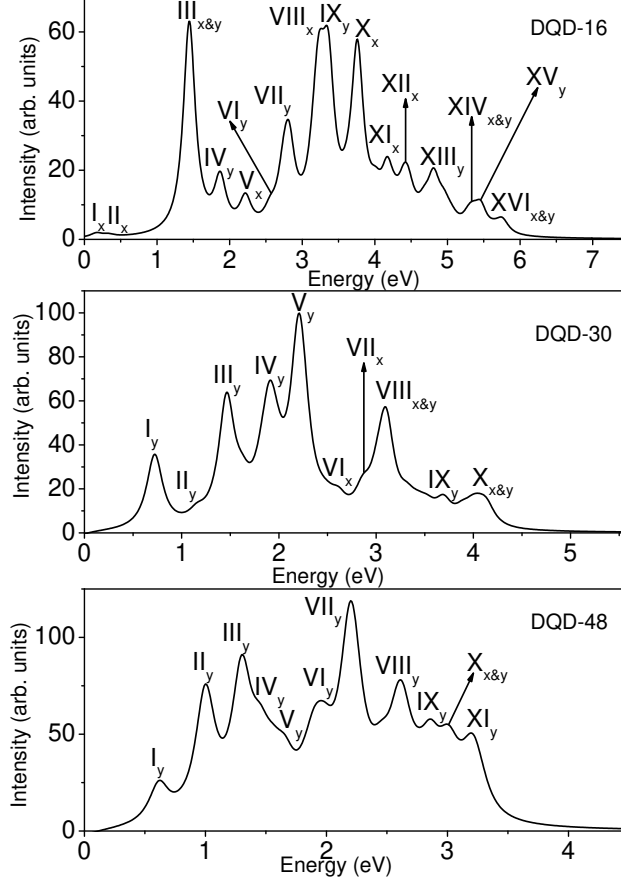


Figure 4: Computed photoinduced absorption spectrum of DQD-16, DQD-30 and DQD-48 with respect to the $1B_{2u}$ state. The subscripts on the peak labels indicate the polarization direction of the absorbed photon.

eV, and single excitations $|H \rightarrow L + 8\rangle - c.c.$ contributing dominantly to its wave function. Hence, it is observed that several states of A_g and B_{1g} symmetries, having energies much greater than the $2A_g$ state, give rise to strong resonances in the PA spectra of these DQDs. It is to be noted that most of the peaks become y -polarized with increase in size of DQD. This is because greater system size in the y direction for larger DQDs leads to increased dominance of y components of the transition dipole matrix elements, over x components. With the increasing size of the DQDs, the PA spectrum overall becomes more intense, due to the larger number of π -electrons in the system. Also noteworthy is that doubly-excited configurations make large contributions to the wave functions of the excited states giving rise to the peaks in the PA spectra, signifying the importance of electron-correlation effects in the description of even-parity states.

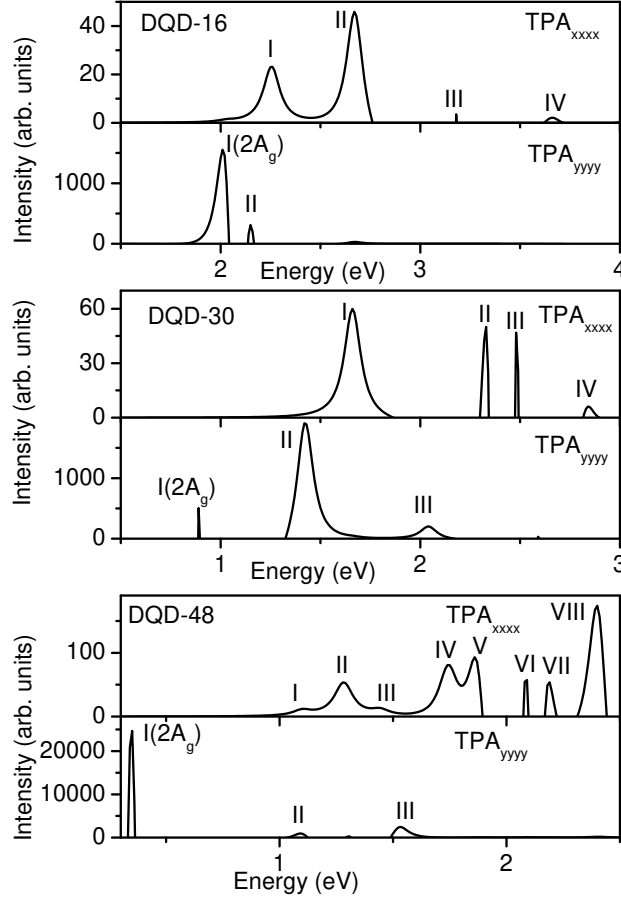


Figure 5: Computed TPA_{xxxx} and TPA_{yyyy} spectra of DQD-16, DQD-30 and DQD-48, at the Hückel level.

2. Two-photon absorption

Fig. 5 represents the two-photon absorption spectra TPA_{xxxx} and TPA_{yyyy} of DQD-16, DQD-30, and DQD-48 at the one-electron (Hückel model) level. The following salient features are observed in the TPA spectra: (i) The TPA spectrum is red-shifted with increasing size of DQDs, analogous to the behavior exhibited by the PA spectrum, (ii) the TPA_{xxxx} component of the spectrum is significantly different as compared to the TPA_{yyyy} component, both qualitatively, and quantitatively, (iii) the resonant intensities of the TPA_{yyyy} component are much larger compared to those of the TPA_{xxxx} component. The reason behind this is that y components of the transition dipole matrix elements are much larger than x components, because of the larger system size in the y direction, (iv) resonant absorption in TPA_{yyyy} occurs at lower energies as compared to the TPA_{xxxx} spectrum. The lowest en-

ergy two-photon peak corresponding to the $2A_g$ state occurs in the TPA_{yyyy} spectrum. For DQD-16, the $2A_g$ peak is due to degenerate single excitations $|H \rightarrow L+3\rangle$ and $|H-3 \rightarrow L\rangle$, while in case of DQD-30 and DQD-48, it corresponds to double excitation $|H \rightarrow L; H \rightarrow L\rangle$, (v) the $2A_g$ peak has the highest intensity for DQD-16, and DQD-48, while the most intense peak for DQD-30, in the TPA_{yyyy} component, corresponds to an mA_g state (a unique state having a strong dipole coupling with $1B_u$ state) located higher than the $2A_g$ state. The mA_g peak of DQD-30 is due to degenerate single excitations $|H \rightarrow L+3\rangle$ and $|H-3 \rightarrow L\rangle$, and (vi) the higher energy peaks in the TPA_{xxxx} component become more intense, with increasing size of DQD.

Now, we present the energies obtained by incorporating electron correlation effects at single configuration interaction (SCI) level with the experimental data for pyrene in Table III. In SCI approach, only one-electron one-hole, i.e., singly-excited configurations with respect to the closed-shell RHF wave function are included. The dominant configurations contributing to the SCI wave functions of important states are given in Table III, and it is observed that the energies obtained from single excitations are in reasonable agreement with the experimental data. However, we note that we obtained much better agreement with the experiments when two-electron two-hole doubly-excited configurations were included at the MRSDCI, and the QCI level (Table. II) for DQD-16. Furthermore, as the electron correlation effects are getting stronger with the increasing sizes of the DQDs, as is evident from the relative $2A_g - 1B_u$ ordering, the SCI method will become progressively worse for these systems as far as the description of two-photon states is concerned. This implies that the two-electron two-hole excitations are essential for quantitatively accurate description of two-photon states.

Next, in fig. 6 we present the two-photon absorptions TPA_{xxxx} , TPA_{yyyy} and TPA_{xyxy} of DQD-16 and DQD-30, respectively, which include the electron-correlation effects at the MRSDCI level. The detailed quantitative information of the various excited states contributing to the TPA spectra of DQD-16 and DQD-30 are listed in the tables S3-S8 of the Supporting Information⁵⁰. Next, we summarize the important features of the TPA/PA spectra of the DQDs, computed at the CI level.

(i) With increasing size of DQDs, the TPA spectrum gets red-shifted, in agreement to the predictions of independent electron level, indicative of band formation. Similarly, the intensity and energy profiles of the peaks are significantly different for TPA_{xxxx} , TPA_{yyyy}

Peak	SCI Results/ Experiment ³⁶ (eV)	Dominant Configurations
A_g	6.46/6.93	$ H - 1 \rightarrow L + 4\rangle + c.c.(0.6995)$
B_{1g}	8.02/8.23	$ H - 7 \rightarrow L\rangle + c.c.(0.5698)$
B_{1g}	8.76/8.57	$ H - 5 \rightarrow L + 4\rangle - c.c.(0.5738)$ $ H - 3 \rightarrow L + 6\rangle + c.c.(0.4034)$
A_g	9.01/9.08	$ H - 1 \rightarrow L + 7\rangle + c.c.(0.6438)$
A_g	9.60/9.22	$ H - 6 \rightarrow L + 4\rangle - c.c.(0.6347)$

Table III: Comparison of the calculated excitation energies (in eV) of the even-parity excited states of DQD-16, contributing to peaks in its TPA spectra, with the experimental data for pyrene³⁶. Note that the two-photon resonances in the absorption spectra are located at half the excitation energies. The calculations were performed at the SCI level, and the dominant configurations contributing to the one electron-hole excitations are also presented.

and TPA_{xyxy} components, due to the fact that different intermediate states contribute to these spectra, (ii) in disagreement with Hückel model results, for DQD-16, the contribution of $2A_g$ state to non-linear susceptibilities is insignificant due to its weak dipole coupling to the B_u state. This is in complete accordance with the PA results discussed earlier. For DQD-30, the $2A_g$ state contributes a very weak peak in the TPA_{yyyy} component of the spectrum, but higher energy A_g states have more intensity. Furthermore, the wave function of the $2A_g$ states are mainly dominated by the double excitation $|H \rightarrow L; H \rightarrow L\rangle$, (iii) the most intense two-photon peaks for DQD-16 and DQD-30 appear in the TPA_{xyxy} component, and correspond to higher energy even parity states with excitation energies 7.38 eV and 4.86 eV, respectively. These states have B_{1g} symmetry, and the double excitations $|H \rightarrow L + 3; H \rightarrow L + 2\rangle - c.c.$ and single excitation $|H - 3 \rightarrow L + 2\rangle + c.c.$ contribute mainly to their many-body wave functions.

Several years back Dixit *et al.*,¹¹ in the context of *trans*-polyacetylene, had argued that the maximum two-photon intensity is not because of the $2A_g$ state, but due to a higher energy even parity state, which they named mA_g , and which has a strong dipole coupling

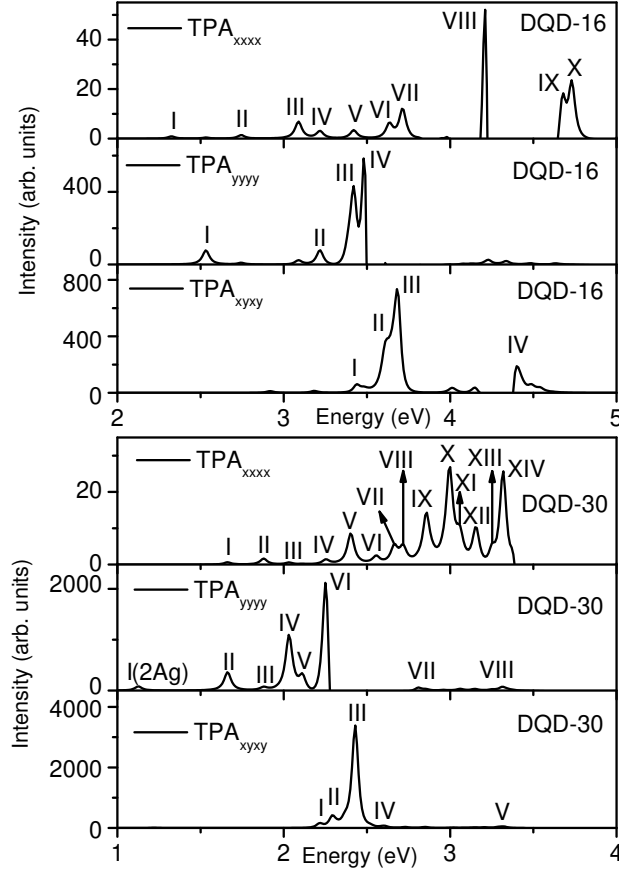


Figure 6: Calculated MRSDCI level TPA_{xxxx} , TPA_{yyyy} and TPA_{xyxy} spectra of DQD-16 and DQD-30.

with the $1B_u$ state. Therefore, such a state will give rise to intense peaks both in TPA as well as in $1B_u$ PA spectra of the system. For other polymers, with more complex structures due to side groups, several states were shown to satisfy mA_g -like properties,^{44,52,56}. In case of DQDs, different TPA components (depending on the selection rules) have either A_g or B_{1g} type two-photon peaks having high intensity, a consequence of their more 2D structure. In order to examine the presence of such generically called mA_g states in DQDs, we do a detailed comparison of their TPA and PA spectra. In case of DQD-16, the states $4A_g$, $5A_g$, $8A_g$, $9A_g$, $10B_{1g}$, $13A_g$, $13B_{1g}$, $24A_g$ and $38A_g$ give rise to intense peaks in PA as well TPA spectra. In particular, the most intense peak in the TPA spectrum is due to $13B_{1g}$ state which also contributes to the strong peak X_x peak in the PA spectrum. In addition, the $13A_g$ state is not only responsible for the most intense peak in the TPA_{yyyy} spectrum, but also gives rise to the second most intense IX_y peak in the PA spectrum. Similarly, the $24A_g$ state

contributes to the highest intensity peak along TPA_{xxxx} component, and the strong $XIII_y$ peak in the PA spectra. For DQD-30, the states $3A_g$, $4A_g$, $5A_g$, $8A_g$, $10A_g$, $12B_{1g}$, $19A_g$, $28A_g$, $34A_g$, $36A_g$ and $34B_{1g}$ lead to strong peaks both in the PA, and the TPA spectra. The $10A_g$ state is responsible for the most intense peak V_y in the PA spectrum, and the fifth strong peak in the TPA_{xxxx} component. Hence, our studies demonstrate that there are many states responsible for strong peaks in the TPA and PA spectra, confirming the existence of several mA_g states in DQDs. In addition, our investigations reveal that unlike a strictly 1D system like *trans*-polyacetylene, the two-photon and photoinduced absorptions in DQDs lead to enhanced nonlinear optical response, with several even parity states contributing to strong absorptions. Based upon the preceding observations for DQD-16 and DQD-30, one can say with confidence that in case of DQD-48 also, the peaks contributing to the PA spectra will also contribute to various components of its TPA spectrum. This shows that TPA and PA spectroscopies are both efficient approaches for probing the two-photon states of these systems.

IV. CONCLUSIONS

In conclusion, our large scale correlated computations employing the PPP Hamiltonian have demonstrated the dominant influence of electron correlation and finite-size effects on the non-linear optical properties of DQDs. Our investigations indicate that the presence of strong electron correlation effects, incorporated within configuration interaction (CI) method, gives rise to reversed excited state ordering in fairly 2D diamond-shaped graphene quantum dots, in contradiction to the results obtained by non-interacting single particle theories. In addition, the role played by electron correlation becomes more conspicuous with increasing size of DQD. However, unlike a strictly 1D system like *trans*-polyacetylene, the non-linear and excited state absorptions in DQDs lead to richer optical properties, with several even parity states contributing to strong absorptions. Therefore, our investigation reveals that both TPA and PA spectroscopies can be utilized to probe the two-photon states of these systems, which are invisible in the linear absorption. We hope that these results will lead to experimental investigations of these systems, paving the way to rational design of graphene-based nonlinear optical devices.

ACKNOWLEDGEMENTS

Work of Tista Basak was supported by DST-SERB, India (Grant No. ECR/2016/000793), while that of A.S. was supported by the DST-SERB, India grant SB/S2/CMP-066/2013.

* Tista.Basak@nmims.edu

† Tushima.Basak@mithibai.ac.in

‡ shukla@phy.iitb.ac.in

- ¹ D. Baeriswyl, D. K. Campbell, and S. Mazumdar, “An overview of the theory of π -conjugated polymers,” in *Conjugated Conducting Polymers. Springer Series in Solid-State Sciences*, edited by H. Kiess (Springer Berlin, Heidelberg, 1992) pp. 7–133.
- ² W. Barford, *Electronic and Optical Properties of Conjugated Polymers*, 2nd ed. (Oxford University Press, 2013).
- ³ F. Wang, G. Dukovic, L. E. Brus, and T. F. Heinz, *Science* **308**, 838 (2005).
- ⁴ N. M. Gabor, Z. Zhong, K. Bosnick, J. Park, and P. L. McEuen, *Science* **325**, 1367 (2009).
- ⁵ P. Sony and A. Shukla, *Synthetic Metals* **155**, 316 (2005), proceedings of the Sixth International Topical Conference on Optical Probes of Conjugated Polymers and Biosystems, Bangalore-INDIA, January 4-8th, 2005.
- ⁶ P. Sony and A. Shukla, *Phys. Rev. B* **75**, 155208 (2007).
- ⁷ T. Basak, H. Chakraborty, and A. Shukla, *Phys. Rev. B* **92**, 205404 (2015).
- ⁸ L. Brus, *Accounts of Chemical Research* **47**, 2951 (2014), pMID: 25120173.
- ⁹ P. C. M. McWilliams, G. W. Hayden, and Z. G. Soos, *Phys. Rev. B* **43**, 9777 (1991).
- ¹⁰ F. Guo, D. Guo, and S. Mazumdar, *Phys. Rev. B* **49**, 10102 (1994).
- ¹¹ S. N. Dixit, D. Guo, and S. Mazumdar, *Phys. Rev. B* **43**, 6781 (1991).
- ¹² R. L. Christensen, M. G. I. Galinato, E. F. Chu, J. N. Howard, R. D. Broene, and H. A. Frank, *The Journal of Physical Chemistry A* **112**, 12629 (2008), pMID: 19007144.
- ¹³ E. Hendry, P. J. Hale, J. Moger, A. K. Savchenko, and S. A. Mikhailov, *Phys. Rev. Lett.* **105**, 097401 (2010).
- ¹⁴ T. Hasan, Z. Sun, F. Wang, F. Bonaccorso, P. H. Tan, A. G. Rozhin, and A. C. Ferrari, *Advanced Materials* **21**, 3874 (2009).

- ¹⁵ Z. Sun, T. Hasan, F. Torrisi, D. Popa, G. Privitera, F. Wang, F. Bonaccorso, D. M. Basko, and A. C. Ferrari, *ACS Nano* **4**, 803 (2010), pMID: 20099874.
- ¹⁶ G. Demetriou, H. T. Bookey, F. Biancalana, E. Abraham, Y. Wang, W. Ji, and A. K. Kar, *Opt. Express* **24**, 13033 (2016).
- ¹⁷ L. Geok-Kheng, C. Zhi-Li, C. Jenny, G. R. G. S., N. Wee-Hao, T. Hong-Wee, F. R. H., H. P. K. H., and C. Lay-Lay, *Nat Photon* **5**, 554 (2011).
- ¹⁸ J. Wang, Y. Hernandez, M. Lotya, J. N. Coleman, and W. J. Blau, *Advanced Materials* **21**, 2430 (2009).
- ¹⁹ X. Cheng, N. Dong, B. Li, X. Zhang, S. Zhang, J. Jiao, W. J. Blau, L. Zhang, and J. Wang, *Opt. Express* **21**, 16486 (2013).
- ²⁰ M. Dragoman, D. Neculoiu, G. Deligeorgis, G. Konstantinidis, D. Dragoman, A. Cismaru, A. A. Muller, and R. Plana, *Applied Physics Letters* **97**, 093101 (2010).
- ²¹ W. Chen, Y. Wang, and W. Ji, *The Journal of Physical Chemistry C* **119**, 16954 (2015).
- ²² J. J. Dean and H. M. van Driel, *Phys. Rev. B* **82**, 125411 (2010).
- ²³ S. Chu, S. Wang, and Q. Gong, *Chemical Physics Letters* **523**, 104 (2012).
- ²⁴ Z. Sun, N. Dong, K. Xie, W. Xia, D. König, T. C. Nagaiah, M. D. Sánchez, P. Ebbinghaus, A. Erbe, X. Zhang, A. Ludwig, W. Schuhmann, J. Wang, and M. Muhler, *The Journal of Physical Chemistry C* **117**, 11811 (2013).
- ²⁵ K. Yoneda, M. Nakano, R. Kishi, H. Takahashi, A. Shimizu, T. Kubo, K. Kamada, K. Ohta, B. Champagne, and E. Botek, *Chemical Physics Letters* **480**, 278 (2009).
- ²⁶ M. K. Brinkley, D. S. L. Abergel, and B. D. Clader, *Journal of Physics: Condensed Matter* **28**, 365001 (2016).
- ²⁷ S. A. Mikhailov, *Phys. Rev. B* **84**, 045432 (2011).
- ²⁸ H. Yang, X. Feng, Q. Wang, H. Huang, W. Chen, A. T. S. Wee, and W. Ji, *Nano Letters* **11**, 2622 (2011).
- ²⁹ J. D. Cox, M. R. Singh, M. A. Antón, and F. Carreño, *Journal of Physics: Condensed Matter* **25**, 385302 (2013).
- ³⁰ S. S. R. K. C. Yamijala, M. Mukhopadhyay, and S. K. Pati, *The Journal of Physical Chemistry C* **119**, 12079 (2015).
- ³¹ S. A. Mikhailov, *Phys. Rev. B* **93**, 085403 (2016).
- ³² X. Feng, X. Li, Z. Li, and Y. Liu, *Opt. Express* **24**, 2877 (2016).

- ³³ K. Aryanpour, A. Shukla, and S. Mazumdar, The Journal of Chemical Physics **140**, 104301 (2014).
- ³⁴ L. A. Agapito, N. Kioussis, and E. Kaxiras, Phys. Rev. B **82**, 201411 (2010).
- ³⁵ T. Basak and A. Shukla, Phys. Rev. B **93**, 235432 (2016).
- ³⁶ P. Salvi, P. Foggi, and E. Castellucci, Chemical Physics Letters **98**, 206 (1983).
- ³⁷ D. C. Elias, R. V. Gorbachev, A. S. Mayorov, S. V. Morozov, A. A. Zhukov, P. Blake, L. A. Ponomarenko, I. V. Grigorieva, K. S. Novoselov, F. Guinea, and A. K. Geim, Nature Physics **7**, 701 (2011).
- ³⁸ J. A. Pople, Trans. Faraday Soc. **49**, 1375 (1953).
- ³⁹ R. Pariser and R. G. Parr, J. Chem. Phys. **21**, 767 (1953).
- ⁴⁰ K. Ohno, Theoretica chimica acta **2**, 219 (1964).
- ⁴¹ M. Chandross and S. Mazumdar, Phys. Rev. B **55**, 1497 (1997).
- ⁴² A. Shukla, Phys. Rev. B **65**, 125204 (2002).
- ⁴³ A. Shukla, Phys. Rev. B **69**, 165218 (2004).
- ⁴⁴ P. Sony and A. Shukla, Phys. Rev. B **71**, 165204 (2005).
- ⁴⁵ P. Sony and A. Shukla, The Journal of Chemical Physics **131**, 014302 (2009).
- ⁴⁶ H. Chakraborty and A. Shukla, The Journal of Physical Chemistry A **117**, 14220 (2013).
- ⁴⁷ H. Chakraborty and A. Shukla, The Journal of Chemical Physics **141**, 164301 (2014).
- ⁴⁸ K. Aryanpour, A. Roberts, A. Sandhu, R. Rathore, A. Shukla, and S. Mazumdar, The Journal of Physical Chemistry C **118**, 3331 (2014).
- ⁴⁹ P. Sony and A. Shukla, Computer Physics Communications **181**, 821 (2010).
- ⁵⁰ Supporting Information.
- ⁵¹ B. Orr and J. Ward, Molecular Physics **20**, 513 (1971).
- ⁵² A. Shukla, Chemical Physics **300**, 177 (2004).
- ⁵³ T. Yumura, K. Kimura, H. Kobayashi, R. Tanaka, N. Okumura, and T. Yamabe, Phys. Chem. Chem. Phys. **11**, 8275 (2009).
- ⁵⁴ G. B. Ray, I. Chakraborty, and S. P. Moulik, Journal of Colloid and Interface Science **294**, 248 (2006).
- ⁵⁵ E. Clar and W. Schmidt, Tetrahedron **34**, 3219 (1978).
- ⁵⁶ A. Shukla, H. Ghosh, and S. Mazumdar, Phys. Rev. B **67**, 245203 (2003).

Supporting Information: Electron correlation effects and two-photon absorption in diamond-shaped graphene quantum dots

Tista Basak^a, Tushima Basak^b, Alok Shukla^{c,d}

^a*Mukesh Patel School of Technology Management and Engineering, NMIMS University, Mumbai 400056, India*

^b*Department of Physics, Mithibai College, Mumbai 400056, India*

^c*Department of Physics, School of Engineering and Applied Sciences, Bennett University, Plot No. 8--11, TechZone II, Greater Noida 201310, Uttar Pradesh, India*

^d*Permanent Address: Department of Physics, Indian Institute of Technology Bombay, Powai, Mumbai 400076, India*

1. Pictorial representation of frontier orbitals

In this section, the pictorial plots of the frontier molecular orbitals H, H-1, H-2, H-3 and H-4 contributing significantly to the non-linear optical properties of DQD-16, DQD-30 and DQD-48 are presented in Figs. S1, S2, and S3, respectively. The expansion coefficients of virtual molecular orbitals L, L+1, L+2, L+3 and L+4 have the same magnitudes (although different relative phases) as those of H, H-1, H-2, H-3 and H-4, respectively, on account of electron-hole symmetry, and hence have not been plotted. The symbols H and L represent the highest occupied molecular orbital (HOMO), and the lowest unoccupied molecular orbital (LUMO), respectively.

*Tista Basak

**Tushima Basak

Alok Shukla

Email addresses: Tista.Basak@nmims.edu (Tista Basak^a), Tushima.Basak@mithibai.ac.in (Tushima Basak^b), shukla@phy.iitb.ac.in (Alok Shukla^{c,d})

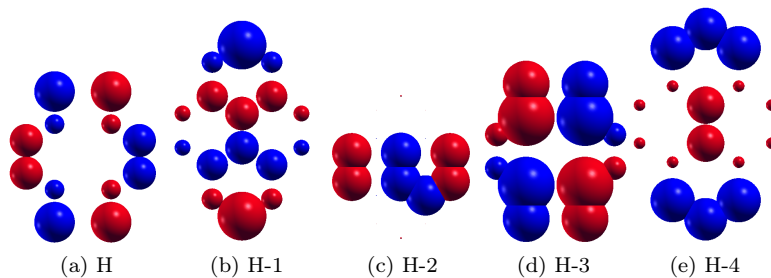


Figure 1: Pictorial representation of the frontier molecular orbitals contributing significantly to the non-linear optical properties of DQD-16. The size of a bubble is proportional to the magnitude of the expansion coefficient at that site (carbon atom), while red/blue colors imply opposite signs of the coefficients. The symbol H represents the highest occupied molecular orbital (HOMO).

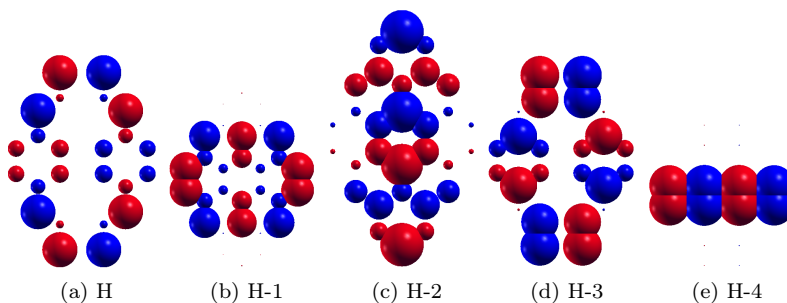


Figure 2: Pictorial representation of the frontier molecular orbitals contributing significantly to the non-linear optical properties of DQD-30. The size of a bubble is proportional to the magnitude of the expansion coefficient at that site (carbon atom), while red/blue colors imply opposite signs of the coefficients. The symbol H represents the highest occupied molecular orbital (HOMO).

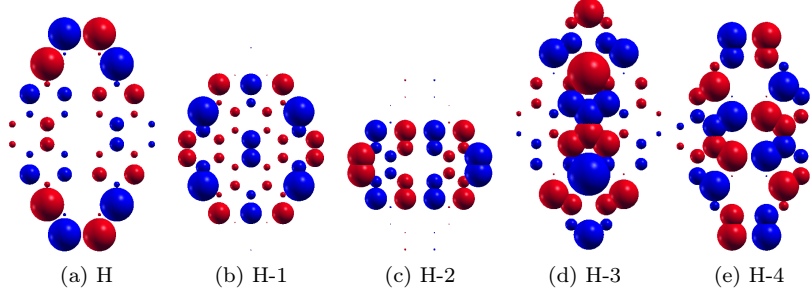


Figure 3: Pictorial representation of the frontier molecular orbitals contributing significantly to the non-linear optical properties of DQD-48. The size of a bubble is proportional to the magnitude of the expansion coefficient at that site (carbon atom), while red/blue colors imply opposite signs of the coefficients. The symbol H represents the highest occupied molecular orbital (HOMO).

In addition, pictorial representation of a closed-shell restricted Hartree-Fock wave-function for a general system is presented in Fig. S4. The mean-field approximation at the restricted Hartree-Fock (RHF) level for a DQD consisting of N carbon atoms (DQD- N), results in $N/2$ doubly occupied, and $N/2$ unoccupied (virtual) molecular orbitals (MOs). A similar graphical representation of configurations contributing to the calculated wave functions, which incorporate electron correlations effects at the CI level, is given in Fig. S5. The symbols H and L represent the highest occupied molecular orbital (HOMO), and the lowest unoccupied molecular orbital (LUMO), respectively. The configurations included in the wave function are interpreted as single-, double-,..., virtual excitations with respect to the restricted Hartree-Fock wave function, and are denoted using arrows from the occupied to unoccupied (virtual) orbitals.

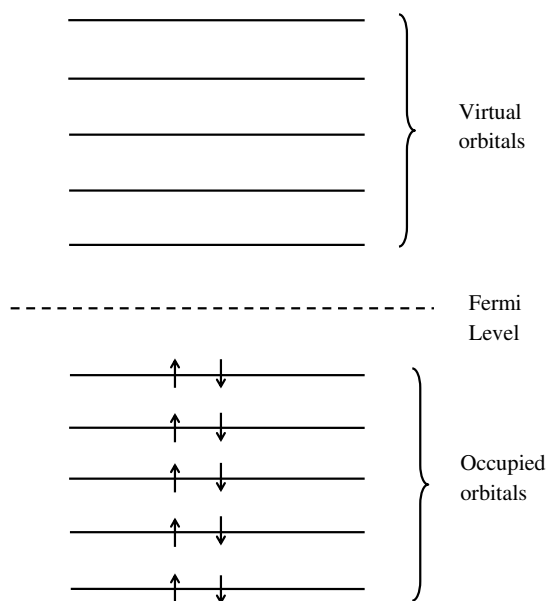


Figure 4: A pictorial representation of the restricted Hartree-Fock wave function of a general molecule, consisting of a few doubly-occupied (filled), and unoccupied (virtual) orbitals. Above, symbol H (L) indicates HOMO (LUMO), while H-n (L+n) denotes n-th orbital below (above) HOMO (LUMO), as shown in the figure.

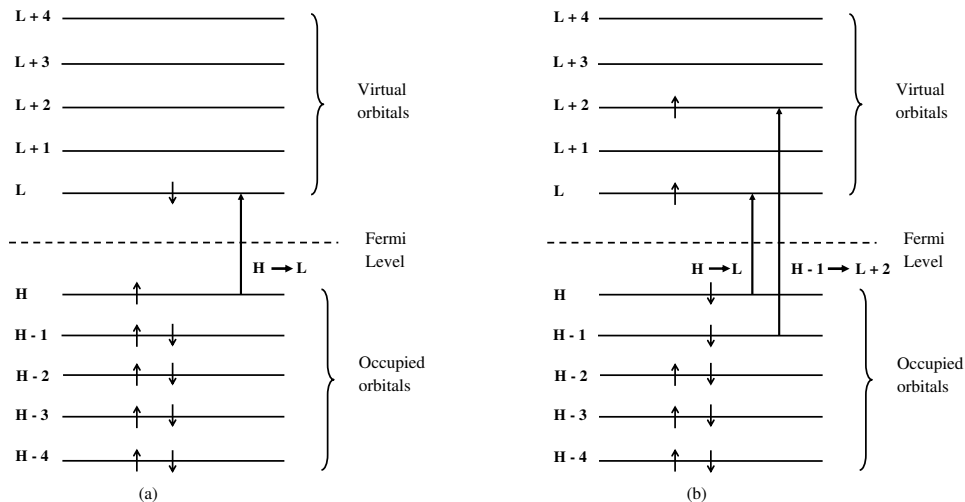


Figure 5: A graphical representation of typical singly- and doubly-excited configurations contributing to the CI wave function of a state (ground or excited) of a molecule: (a) a singly excited configuration obtained by promoting one electron from the HOMO to the LUMO, denoted as $|H \rightarrow L\rangle$ and (b) a doubly-excited configuration obtained by promoting one electron from HOMO to LUMO, and another one from HOMO-1 to the LUMO+2 orbital, and denoted as $|H \rightarrow L; H-1 \rightarrow L+2\rangle$. The symbols H and L represent the HOMO, and the LUMO, respectively. The arrows represent virtual excitations from the occupied to virtual orbitals. In reality, the configurations are composed of properly anti-symmetrized Slater determinants.

2. Dimensions of CI matrices

In this section, we present the dimensions of the CI matrices employed for the computation of excited state ordering and two-photon absorption spectrum of DQD-16, DQD-30 and DQD-48. For excited state ordering calculation, the first two lowest energy two-photon states ($1A_g$ and $2A_g$) and first one-photon ($1B_{2u}$) state was optimized at the quadratic configuration interaction (QCI) level for DQD-16, while multi-reference singles-doubles configuration interaction (MRSDCI) methodology was adopted for DQD-30 and DQD-48. The dimensions of the resultant CI matrices for A_g and B_{2u} symmetries for DQD-16, DQD-30 and DQD-48 are given in Table S1.

Table S1: Dimensions of the CI matrices for A_g and B_{2u} symmetries for excited state ordering computation for DQD-16, DQD-30 and DQD-48.

System	Dimension of CI matrix	
	A_g	B_{2u}
DQD-16	73857	126279
DQD-30	2896621	2737260
DQD-48	17903219	12424745

For computing the two-photon absorption (TPA) and photoinduced absorption (PA) spectra, the maximum energy limit of the excited states was restricted to 10 eV for CI calculations. The QCI method was used for the A_g and the B_{2u} states of DQD-16. The MRSDCI approach was adopted for the B_{3u} and the B_{1g} symmetries of DQD-16. Further, the MRSDCI methodology was considered for optimizing all the symmetries of DQD-30 and DQD-48. The dimensions of CI matrices of A_g , B_{1g} , B_{2u} and B_{3u} symmetries considered for the computation of TPA spectra of DQD-16 and DQD-30 are given in the table S2. In case of the computation of PA spectra of DQD-16, DQD-30 and DQD-48, the size of the CI matrix for computing the first optically excited $1B_{2u}$ state is also given in the table.

Table S2: Dimensions of CI matrices of A_g , B_{1g} , B_{2u} and B_{3u} symmetries for the computation of TPA and PA spectra of DQD-16, DQD-30 and DQD-48.

Symmetry	Dimension of CI matrix		
	DQD-16	DQD-30	DQD-48
A_g	73857	2274042	10252792
B_{1g}	153690	1803596	10337444
B_{2u}	126279	1564554	—
B_{3u}	127304	1359014	—
$1B_{2u}$	126279	152637	702796

3. Computed energies and wave functions of the excited states contributing to the non-linear absorption spectra

In this section, the dominant wave-function and energies of different excited states contributing to TPA_{xxxx} , TPA_{yyyy} and TPA_{xyxy} components of the two photon absorption spectrum for DQD-16 and DQD-30 are listed in tables S3, S4, S5, S6, S7 and S8. The calculations have been done at the QCI level for A_g and B_{2u} symmetry states, and MRSDCI level for B_{1g} and B_{3u} states for DQD-16. However, for DQD-30 and DQD-48, the calculations for all symmetries have been done at the MRSDCI level. The abbreviation “c.c.” represents coefficient

of charge conjugate of a given singly excited configuration while the sign (+/−) preceding “c.c.” implies that the two coefficients have (same/opposite) signs. In case of possibility of more than one charge-conjugate counterparts, each with its own sign, no +/− sign precedes c.c. The symbol $|H \rightarrow L\rangle$ implies singly excited configuration obtained by promoting one electron from HOMO to LUMO, with respect to the closed-shell Hartree-Fock reference state. Similarly, one can deduce the meaning of other singly-excited configurations such as $|H - 1 \rightarrow L + 2\rangle$ etc. The symbol $|H \rightarrow L; H - 1 \rightarrow L + 1\rangle$ denotes a doubly-excited configuration obtained by exciting two electrons from the Hartree-Fock reference state, one from HOMO to LUMO, the other one from HOMO-1 to LUMO+1. Nature of other doubly-excited configurations can also be deduced, similarly.

Table S3: Excited states contributing to TPA_{xxx} component of the two photon absorption spectrum of DQD-16, computed employing QCI and MRSDCI approaches. The 2^1A_g state does not give rise to a peak in the TPA spectrum.

Peak	State	E (eV)	Dominant Configurations
-	2^1A_g	3.68	$ H \rightarrow L; H \rightarrow L\rangle(0.5109)$ $ H - 3 \rightarrow L\rangle - c.c.(0.4084)$
<i>I</i>	3^1A_g	4.65	$ H - 1 \rightarrow L + 2\rangle - c.c.(0.5294)$ $ H \rightarrow L; H - 1 \rightarrow L + 1\rangle(0.2088)$
<i>II</i>	5^1A_g	5.49	$ H - 1 \rightarrow L + 4\rangle + c.c.(0.4732)$ $ H - 1 \rightarrow L + 1; H - 1 \rightarrow L + 1\rangle(0.2681)$
<i>III</i>	8^1A_g	6.18	$ H \rightarrow L; H - 1 \rightarrow L + 1\rangle(0.5066)$ $ H \rightarrow L; H - 5 \rightarrow L\rangle + c.c.(0.2352)$
<i>IV</i>	9^1A_g	6.44	$ H - 2 \rightarrow L + 2; H \rightarrow L\rangle(0.3801)$ $ H \rightarrow L; H \rightarrow L\rangle(0.2878)$ $ H \rightarrow L; H - 1 \rightarrow L + 1\rangle(0.2773)$
<i>V</i>	11^1A_g	6.84	$ H \rightarrow L; H - 2 \rightarrow L + 2\rangle(0.2734)$ $ H \rightarrow L; H - 1 \rightarrow L + 1\rangle(0.2448)$ $ H - 2 \rightarrow L; H - 2 \rightarrow L\rangle + c.c.(0.2159)$
<i>VI</i>	14^1A_g	7.27	$ H \rightarrow L; H - 2 \rightarrow L + 2\rangle(0.3199)$ $ H - 1 \rightarrow L + 7\rangle + c.c.(0.2022)$ $ H - 2 \rightarrow L + 1; H - 1 \rightarrow L + 2\rangle(0.1882)$ $ H \rightarrow L; H - 1 \rightarrow L + 1\rangle(0.1827)$
<i>VII</i>	15^1A_g	7.43	$ H - 1 \rightarrow L + 7\rangle + c.c.(0.3022)$ $ H - 2 \rightarrow L + 1; H - 1 \rightarrow L + 2\rangle(0.2246)$ $ H \rightarrow L; H - 1 \rightarrow L + 1\rangle(0.2121)$
<i>VIII</i>	24^1A_g	8.43	$ H \rightarrow L; H - 1 \rightarrow L + 1\rangle(0.2572)$ $ H \rightarrow L + 3; H - 3 \rightarrow L\rangle(0.1979)$ $ H - 2 \rightarrow L + 1; H - 1 \rightarrow L + 2\rangle(0.1932)$ $ H \rightarrow L; H - 4 \rightarrow L + 4\rangle(0.1767)$ $ H - 4 \rightarrow L + 2; H - 2 \rightarrow L + 4\rangle(0.1736)$
<i>IX</i>	38^1A_g	9.35	$ H - 2 \rightarrow L + 2; H - 2 \rightarrow L + 2\rangle(0.2020)$ $ H - 2 \rightarrow L; H - 2 \rightarrow L\rangle + c.c.(0.1916)$ $ H \rightarrow L; H - 2 \rightarrow L + 2\rangle(0.1770)$ $ H - 2 \rightarrow L + 2; H - 5 \rightarrow L\rangle - c.c.(0.1683)$
<i>X</i>	40^1A_g	9.46	$ H \rightarrow L; H - 4 \rightarrow L + 4\rangle(0.2160)$ $ H \rightarrow L + 3; H - 3 \rightarrow L\rangle(0.2057)$ $ H \rightarrow L + 3; H - 1 \rightarrow L + 4\rangle - c.c.(0.1580)$ $ H - 2 \rightarrow L + 3; H - 1 \rightarrow L\rangle + c.c.(0.1544)$

Table S4: Excited states contributing to TPA_{yyyy} component of the two photon absorption spectrum of DQD-16, computed employing QCI and MRSDCI approaches.

Peak	State	E (eV)	Dominant Configurations
<i>I</i>	4^1A_g	5.06	$ H \rightarrow L; H \rightarrow L\rangle(0.4372)$ $ H - 2 \rightarrow L + 2; H \rightarrow L\rangle(0.3465)$ $ H - 3 \rightarrow L\rangle - c.c.(0.3275)$
<i>II</i>	9^1A_g	6.44	$ H - 2 \rightarrow L + 2; H \rightarrow L\rangle(0.3801)$ $ H \rightarrow L; H \rightarrow L\rangle(0.2878)$ $ H \rightarrow L; H - 1 \rightarrow L + 1\rangle(0.2773)$
<i>III</i>	11^1A_g	6.84	$ H \rightarrow L; H - 2 \rightarrow L + 2\rangle(0.2734)$ $ H \rightarrow L; H - 1 \rightarrow L + 1\rangle(0.2448)$ $ H - 2 \rightarrow L; H - 2 \rightarrow L\rangle + c.c.(0.2159)$
<i>IV</i>	13^1A_g	6.98	$ H - 1 \rightarrow L; H - 1 \rightarrow L\rangle + c.c.(0.3367)$ $ H \rightarrow L; H - 1 \rightarrow L + 1\rangle(0.2960)$ $ H \rightarrow L; H - 2 \rightarrow L + 2\rangle(0.2176)$

Table S5: Excited states contributing to TPA_{xyxy} component of the two photon absorption spectrum of DQD-16, computed employing QCI and MRSDCI approaches.

Peak	State	E (eV)	Dominant Configurations
<i>I</i>	10^1B_{1g}	6.87	$ H - 2 \rightarrow L + 5\rangle + c.c.(0.3527)$ $ H \rightarrow L + 7\rangle + c.c.(0.2039)$
<i>II</i>	12^1B_{1g}	7.22	$ H - 4 \rightarrow L + 5\rangle - c.c.(0.2980)$ $ H \rightarrow L; H - 6 \rightarrow L\rangle + c.c.(0.2031)$
<i>III</i>	13^1B_{1g}	7.38	$ H \rightarrow L + 3; H \rightarrow L + 2\rangle - c.c.(0.2672)$ $ H \rightarrow L + 2\rangle - c.c.(0.1797)$
<i>IV</i>	27^1B_{1g}	8.75	$ H - 5 \rightarrow L + 4\rangle - c.c.(0.2345)$ $ H \rightarrow L + 2; H - 3 \rightarrow L\rangle c.c.(0.1815)$

Table S6: Excited states contributing to TPA_{xxx} component of two photon absorption spectrum of DQD-30, computed employing MRSDCI approach.

Peak	State	E (eV)	Dominant Configurations
<i>I</i>	3^1A_g	3.32	$ H-1 \rightarrow L+1; H \rightarrow L\rangle(0.3786)$ $ H \rightarrow L+3\rangle - c.c.(0.3669)$ $ H \rightarrow L; H-7 \rightarrow L\rangle + c.c.(0.2233)$
<i>II</i>	4^1A_g	3.76	$ H-1 \rightarrow L+1; H \rightarrow L\rangle(0.4052)$ $ H-2 \rightarrow L+1\rangle + c.c.(0.3708)$ $ H-1 \rightarrow L; H-1 \rightarrow L\rangle + c.c.(0.2293)$
<i>III</i>	5^1A_g	4.06	$ H-4 \rightarrow L; H \rightarrow L\rangle - c.c.(0.3451)$ $ H \rightarrow L; H \rightarrow L\rangle(0.2952)$ $ H-1 \rightarrow L+1; H \rightarrow L\rangle(0.2577)$
<i>IV</i>	8^1A_g	4.51	$ H-10 \rightarrow L\rangle - c.c.(0.3163)$ $ H \rightarrow L; H \rightarrow L+7\rangle + c.c.(0.2521)$
<i>V</i>	10^1A_g	4.81	$ H-1 \rightarrow L+1; H \rightarrow L\rangle(0.3394)$ $ H \rightarrow L; H \rightarrow L+4\rangle - c.c.(0.2895)$
<i>VI</i>	13^1A_g	5.11	$ H-2 \rightarrow L+5\rangle + c.c.(0.2628)$ $ H-6 \rightarrow L+1\rangle + c.c.(0.2231)$
<i>VII</i>	14^1A_g	5.33	$ H-4 \rightarrow L; H \rightarrow L+4\rangle(0.4188)$ $ H \rightarrow L; H-1 \rightarrow L+9\rangle + c.c.(0.2556)$
<i>VIII</i>	16^1A_g	5.43	$ H \rightarrow L; H-2 \rightarrow L+2\rangle(0.3961)$ $ H-2 \rightarrow L+5\rangle + c.c.(0.2383)$
<i>IX</i>	19^1A_g	5.71	$ H \rightarrow L; H-2 \rightarrow L+2\rangle(0.4582)$ $ H-1 \rightarrow L+1; H \rightarrow L\rangle(0.1968)$
<i>X</i>	22^1A_g	5.99	$ H-5 \rightarrow L+1; H \rightarrow L\rangle + c.c.(0.2582)$ $ H-4 \rightarrow L+3\rangle - c.c.(0.2561)$ $ H \rightarrow L; H-2 \rightarrow L+2\rangle(0.2557)$
<i>XI</i>	24^1A_g	6.11	$ H-1 \rightarrow L+1; H \rightarrow L+4\rangle + c.c.(0.3335)$ $ H-1 \rightarrow L+1; H-1 \rightarrow L+1\rangle(0.3331)$
<i>XII</i>	28^1A_g	6.30	$ H-6 \rightarrow L+5\rangle + c.c.(0.2660)$ $ H \rightarrow L+2; H \rightarrow L+6\rangle - c.c.(0.2158)$
	30^1A_g	6.31	$ H \rightarrow L; H-2 \rightarrow L+6\rangle + c.c.(0.2592)$ $ H \rightarrow L; H-5 \rightarrow L+1\rangle + c.c.(0.1626)$
<i>XIII</i>	32^1A_g	6.50	$ H \rightarrow L; H-4 \rightarrow L+4\rangle(0.2656)$ $ H-1 \rightarrow L+1; H-1 \rightarrow L+1\rangle(0.2007)$
<i>XIV</i>	36^1A_g	6.64	$ H \rightarrow L; H-2 \rightarrow L+6\rangle + c.c.(0.2281)$ $ H-9 \rightarrow L+2\rangle + c.c.(0.2196)$

Table S7: Excited states contributing to TPA_{yyyy} component of the two photon absorption spectrum of DQD-30, computed employing MRSDCI approach.

Peak	State	E (eV)	Dominant Configurations
<i>I</i>	2^1A_g	2.25	$ H \rightarrow L; H \rightarrow L\rangle(0.6332)$ $ H \rightarrow L + 3\rangle - c.c.(0.2902)$
<i>II</i>	3^1A_g	3.32	$ H - 1 \rightarrow L + 1; H \rightarrow L\rangle(0.3786)$ $ H \rightarrow L + 3\rangle - c.c.(0.3669)$ $ H \rightarrow L; H - 7 \rightarrow L\rangle + c.c.(0.2233)$
<i>III</i>	4^1A_g	3.76	$ H - 1 \rightarrow L + 1; H \rightarrow L\rangle(0.4052)$ $ H - 2 \rightarrow L + 1\rangle + c.c.(0.3708)$ $ H - 1 \rightarrow L; H - 1 \rightarrow L\rangle + c.c.(0.2293)$
<i>IV</i>	5^1A_g	4.06	$ H - 4 \rightarrow L; H \rightarrow L\rangle - c.c.(0.3451)$ $ H \rightarrow L; H \rightarrow L\rangle(0.2952)$ $ H - 1 \rightarrow L + 1; H \rightarrow L\rangle(0.2577)$
<i>V</i>	6^1A_g	4.23	$ H - 1 \rightarrow L + 2\rangle + c.c.(0.3315)$ $ H \rightarrow L; H - 1 \rightarrow L + 1\rangle(0.2389)$ $ H \rightarrow L + 1; H \rightarrow L + 1\rangle + c.c.(0.2243)$
<i>VI</i>	8^1A_g	4.51	$ H - 10 \rightarrow L\rangle - c.c.(0.3163)$ $ H \rightarrow L; H \rightarrow L + 7\rangle + c.c.(0.2521)$
<i>VII</i>	17^1A_g	5.62	$ H - 1 \rightarrow L + 8\rangle + c.c.(0.2370)$ $ H - 4 \rightarrow L + 3\rangle - c.c.(0.1872)$ $ H - 5 \rightarrow L; H - 1 \rightarrow L\rangle - c.c.(0.1803)$
<i>VIII</i>	34^1A_g	6.63	$ H - 1 \rightarrow L + 1; H \rightarrow L\rangle(0.2317)$ $ H \rightarrow L + 3; H - 3 \rightarrow L\rangle(0.2312)$ $ H \rightarrow L; H - 6 \rightarrow L + 6\rangle(0.2246)$ $ H - 9 \rightarrow L + 2\rangle + c.c.(0.2012)$
	36^1A_g	6.64	$ H \rightarrow L; H - 2 \rightarrow L + 6\rangle + c.c.(0.2281)$ $ H - 9 \rightarrow L + 2\rangle + c.c.(0.2196)$ $ H \rightarrow L + 2; H \rightarrow L + 2\rangle + c.c.(0.2058)$

Table S8: Excited states contributing to TPA_{xyxy} component of the two photon absorption spectrum of DQD-30, computed employing MRSDCI approach.

Peak	State	E (eV)	Dominant Configurations
<i>I</i>	5^1B_{1g}	4.43	$ H \rightarrow L; H - 6 \rightarrow L\rangle + c.c.(0.2754)$ $ H - 9 \rightarrow L\rangle - c.c.(0.2634)$ $ H \rightarrow L; H \rightarrow L + 2\rangle + c.c.(0.2380)$
<i>II</i>	6^1B_{1g}	4.58	$ H \rightarrow L; H \rightarrow L + 6\rangle + c.c.(0.3054)$ $ H \rightarrow L; H \rightarrow L + 2\rangle + c.c.(0.2953)$ $ H - 3 \rightarrow L + 2\rangle + c.c.(0.1985)$
<i>III</i>	9^1B_{1g}	4.86	$ H - 3 \rightarrow L + 2\rangle + c.c.(0.3156)$ $ H - 1 \rightarrow L + 4\rangle - c.c.(0.2421)$ $ H \rightarrow L + 1\rangle - c.c.(0.2372)$
<i>IV</i>	12^1B_{1g}	5.21	$ H - 9 \rightarrow L\rangle - c.c.(0.3308)$ $ H - 1 \rightarrow L; H - 2 \rightarrow L + 1\rangle - c.c.(0.1894)$
<i>V</i>	34^1B_{1g}	6.65	$ H \rightarrow L + 1; H - 6 \rightarrow L + 1\rangle + c.c.(0.2532)$ $ H - 1 \rightarrow L; H - 6 \rightarrow L + 1\rangle c.c.(0.1818)$ $ H - 1 \rightarrow L + 7\rangle + c.c.(0.1718)$ $ H - 5 \rightarrow L + 7\rangle + c.c.(0.1564)$

4. Computed energies and wave functions of the excited states contributing to the photoinduced absorption spectra

In this section, the dominant wave-function and energies of the different excited states contributing to the photoinduced absorption spectra for DQD-16, DQD-30 and DQD-48 are listed in tables S9, S10 and S11. These tables represent the positions of the peaks from the $1B_{2u}$ state and the dominant wave-functions of the excited states contributing to these peaks. The abbreviation “c.c.” represents coefficient of charge conjugate of a given singly excited configuration while the sign (+/−) preceding “c.c.” implies that the two coefficients have (same/opposite) signs. In case of possibility of more than one charge-conjugate counterparts, each with its own sign, no +/− sign precedes c.c.

Table S9: Excited states contributing to the $1B_{2u}$ photoinduced absorption spectrum of DQD-16.

Peak	State	E (eV)	Dominant Configurations
-	2^1A_g		
I_x	1^1B_{1g}	3.78	$ H \rightarrow L + 2\rangle - c.c. (0.5495)$ $ H \rightarrow L + 2; H - 3 \rightarrow L\rangle c.c. (0.1573)$
II_x	2^1B_{1g}	3.95	$ H \rightarrow L + 4\rangle + c.c. (0.4862)$ $ H \rightarrow L + 1; H \rightarrow L\rangle - c.c. (0.2527)$
$III_{x\&y}$	4^1A_g	5.06	$ H \rightarrow L; H \rightarrow L\rangle (0.4372)$ $ H - 2 \rightarrow L + 2; H \rightarrow L\rangle (0.3465)$
	4^1B_{1g}	5.07	$ H - 1 \rightarrow L + 3\rangle - c.c. (0.5071)$ $ H - 1 \rightarrow L; H \rightarrow L\rangle - c.c. (0.2065)$
IV_y	5^1A_g	5.49	$ H - 1 \rightarrow L + 4\rangle + c.c. (0.4732)$ $ H - 1 \rightarrow L + 1; H - 1 \rightarrow L + 1\rangle (0.2681)$
V_x	6^1B_{1g}	5.84	$ H - 1 \rightarrow L; H \rightarrow L\rangle - c.c. (0.3211)$ $ H \rightarrow L + 3; H \rightarrow L + 2\rangle - c.c. (0.2153)$ $ H - 4 \rightarrow L\rangle + c.c. (0.1931)$
VI_y	8^1A_g	6.18	$ H \rightarrow L + 1; H - 1 \rightarrow L\rangle (0.5066)$ $ H - 5 \rightarrow L; H \rightarrow L\rangle + c.c. (0.2352)$
VII_y	9^1A_g	6.44	$ H - 2 \rightarrow L + 2; H \rightarrow L\rangle (0.3801)$ $ H \rightarrow L; H \rightarrow L\rangle (0.2878)$
$VIII_x$	10^1B_{1g}	6.87	$ H - 2 \rightarrow L + 5\rangle + c.c. (0.3527)$ $ H \rightarrow L + 7\rangle + c.c. (0.2039)$ $ H - 5 \rightarrow L + 1; H \rightarrow L\rangle c.c. (0.1953)$
IX_y	13^1A_g	6.98	$ H - 1 \rightarrow L; H - 1 \rightarrow L\rangle + c.c. (0.3367)$ $ H \rightarrow L; H - 1 \rightarrow L + 1\rangle (0.2960)$ $ H \rightarrow L; H - 2 \rightarrow L + 2\rangle (0.2176)$

Peak	State	E (eV)	Dominant Configurations
X_x	13^1B_{1g}	7.38	$ H \rightarrow L + 3; H \rightarrow L + 2\rangle - c.c. (0.2672)$ $ H \rightarrow L + 2\rangle - c.c. (0.1797)$ $ H \rightarrow L + 3; H - 2 \rightarrow L\rangle c.c. (0.1546)$
XI_x	16^1B_{1g}	7.79	$ H \rightarrow L + 1; H - 1 \rightarrow L + 1\rangle - c.c. (0.2406)$ $ H - 4 \rightarrow L + 1; H \rightarrow L + 2\rangle c.c. (0.2209)$ $ H - 2 \rightarrow L + 1; H - 4 \rightarrow L\rangle - c.c. (0.1581)$
XII_x	17^1B_{1g}	8.02	$ H - 1 \rightarrow L; H - 1 \rightarrow L + 1\rangle - c.c. (0.2721)$ $ H - 1 \rightarrow L + 2; H - 2 \rightarrow L\rangle c.c. (0.2037)$ $ H \rightarrow L + 2; H - 3 \rightarrow L\rangle c.c. (0.1693)$
$XIII_y$	24^1A_g	8.43	$ H - 1 \rightarrow L; H \rightarrow L + 1\rangle (0.2572)$ $ H - 3 \rightarrow L; H \rightarrow L + 3\rangle (0.1979)$ $ H - 2 \rightarrow L + 1; H - 1 \rightarrow L + 2\rangle (0.1932)$
$XIV_{x\&y}$	32^1A_g	8.97	$ H - 1 \rightarrow L + 1; H - 3 \rightarrow L + 3\rangle (0.1826)$ $ H \rightarrow L + 1; H - 3 \rightarrow L + 4\rangle - c.c. (0.1608)$ $ H - 1 \rightarrow L + 4; H - 3 \rightarrow L\rangle - c.c. (0.1540)$
	30^1B_{1g}	8.97	$ H - 2 \rightarrow L + 1; H - 4 \rightarrow L\rangle - c.c. (0.2226)$ $ H - 2 \rightarrow L; H \rightarrow L + 3\rangle c.c. (0.1738)$ $ H - 4 \rightarrow L + 5\rangle - c.c. (0.1180)$

Peak	State	E (eV)	Dominant Configurations
XV_y	33^1A_g	9.04	$ H - 3 \rightarrow L + 4; H \rightarrow L + 1\rangle - c.c. (0.2192)$ $ H - 5 \rightarrow L; H \rightarrow L\rangle + c.c. (0.1885)$
$XVI_{x\&y}$	38^1A_g	9.35	$ H - 2 \rightarrow L + 2; H - 2 \rightarrow L + 2\rangle (0.2020)$ $ H - 2 \rightarrow L; H - 2 \rightarrow L\rangle + c.c. (0.1916)$ $ H - 2 \rightarrow L + 2; H \rightarrow L\rangle (0.1770)$
	37^1B_{1g}	9.38	$ H \rightarrow L + 2; H \rightarrow L + 2; H - 2 \rightarrow L\rangle - c.c. (0.2102)$ $ H - 2 \rightarrow L + 5\rangle + c.c. (0.1817)$ $ H \rightarrow L; H \rightarrow L; H - 5 \rightarrow L + 2\rangle + c.c. (0.1402)$

Table S10: Excited states contributing to the $1B_{2u}$ photoinduced absorption spectrum of DQD-30.

Peak	State	E (eV)	Dominant Configurations
I_y	3^1A_g	3.32	$ H - 1 \rightarrow L + 1; H \rightarrow L\rangle(0.3786)$ $ H \rightarrow L + 3\rangle - c.c.(0.3669)$
II_y	4^1A_g	3.76	$ H - 1 \rightarrow L + 1; H \rightarrow L\rangle(0.4052)$ $ H - 2 \rightarrow L + 1\rangle + c.c.(0.3708)$
III_y	5^1A_g	4.06	$ H - 4 \rightarrow L; H \rightarrow L\rangle - c.c.(0.3451)$ $ H \rightarrow L; H \rightarrow L\rangle(0.2952)$
IV_y	8^1A_g	4.51	$ H - 10 \rightarrow L\rangle - c.c.(0.3163)$ $ H \rightarrow L + 7; H \rightarrow L\rangle + c.c.(0.2521)$ $ H \rightarrow L + 3; H - 3 \rightarrow L\rangle(0.2076)$
V_y	10^1A_g	4.81	$ H - 1 \rightarrow L + 1; H \rightarrow L\rangle(0.3394)$ $ H \rightarrow L + 4; H \rightarrow L\rangle - c.c.(0.2895)$
VI_x	12^1B_{1g}	5.21	$ H - 9 \rightarrow L\rangle - c.c.(0.3308)$ $ H - 1 \rightarrow L; H - 2 \rightarrow L + 1\rangle c.c.(0.1894)$ $ H - 11 \rightarrow L\rangle + c.c.(0.1533)$

Peak	State	E (eV)	Dominant Configurations
VII_x	14^1B_{1g}	5.46	$ H \rightarrow L + 11\rangle + c.c.(0.2115)$ $ H - 1 \rightarrow L; H - 2 \rightarrow L + 1\rangle c.c.(0.2016)$ $ H - 1 \rightarrow L + 7\rangle + c.c.(0.1887)$
$VIII_{x\&y}$	17^1B_{1g}	5.70	$ H - 1 \rightarrow L; H \rightarrow L + 1; H \rightarrow L + 1\rangle - c.c.(0.2382)$ $ H - 3 \rightarrow L + 2\rangle + c.c.(0.2271)$ $ H - 1 \rightarrow L; H - 3 \rightarrow L\rangle - c.c.(0.2072)$
	19^1A_g	5.71	$ H \rightarrow L; H - 2 \rightarrow L + 2\rangle(0.4582)$ $ H - 1 \rightarrow L + 1; H \rightarrow L\rangle(0.1968)$
IX_y	28^1A_g	6.30	$ H - 6 \rightarrow L + 5\rangle + c.c.(0.2660)$ $ H \rightarrow L + 2; H \rightarrow L + 6\rangle - c.c.(0.2158)$ $ H - 4 \rightarrow L; H \rightarrow L + 4\rangle(0.1843)$
$X_{x\&y}$	34^1B_{1g}	6.65	$ H \rightarrow L + 1; H - 6 \rightarrow L + 1\rangle + c.c.(0.2532)$ $ H - 1 \rightarrow L; H - 6 \rightarrow L + 1\rangle c.c.(0.1818)$ $ H - 1 \rightarrow L + 7\rangle + c.c.(0.1718)$
	34^1A_g	6.63	$ H - 1 \rightarrow L + 1; H \rightarrow L\rangle(0.2317)$ $ H \rightarrow L + 3; H - 3 \rightarrow L\rangle(0.2312)$ $ H \rightarrow L; H - 6 \rightarrow L + 6\rangle(0.2246)$ $ H - 9 \rightarrow L + 2\rangle + c.c.(0.2012)$
	36^1A_g	6.64	$ H \rightarrow L; H - 2 \rightarrow L + 6\rangle + c.c.(0.2281)$ $ H - 9 \rightarrow L + 2\rangle + c.c.(0.2196)$ $ H \rightarrow L + 2; H \rightarrow L + 2\rangle + c.c.(0.2058)$

Table S11: Excited states contributing to the $1B_{2u}$ photoinduced absorption spectrum of DQD-48.

Peak	State	E (eV)	Dominant Configurations
I_y	4^1A_g	2.60	$ H-1 \rightarrow L+1\rangle(0.4402)$ $ H \rightarrow L+1; L \rightarrow L+1\rangle+c.c.(0.3217)$
II_y	5^1A_g	2.99	$ H \rightarrow L+2\rangle-c.c.(0.3116)$ $ L \rightarrow L+4\rangle-c.c.(0.3050)$
III_y	7^1A_g	3.29	$ H-1 \rightarrow H; H-1 \rightarrow L+1; L \rightarrow L+1\rangle(0.3717)$ $ H \rightarrow L+2\rangle-c.c.(0.3177)$
IV_y	8^1A_g	3.44	$ H-3 \rightarrow H; L \rightarrow L+1\rangle-c.c.(0.3341)$ $ H-2 \rightarrow L+2\rangle(0.2758)$
V_y	11^1A_g	3.64	$ H-2 \rightarrow L+2\rangle(0.2575)$ $ H-12 \rightarrow H\rangle+c.c.(0.2432)$
VI_y	14^1A_g	3.95	$ H-5 \rightarrow H; L \rightarrow L+1\rangle-c.c.(0.2566)$ $ H-1 \rightarrow H; H-1 \rightarrow L+1; L \rightarrow L+1\rangle(0.2385)$
VII_y	16^1A_g	4.19	$ H \rightarrow L+8\rangle-c.c.(0.3148)$ $ H-5 \rightarrow H; L \rightarrow L+1\rangle-c.c.(0.2625)$
$VIII_y$	22^1A_g	4.58	$ H-1 \rightarrow H; H-1 \rightarrow L+1; L \rightarrow L+1\rangle(0.2463)$ $ H-1 \rightarrow L+10\rangle-c.c.(0.2103)$
IX_y	27^1A_g	4.85	$ H-1 \rightarrow L+1\rangle(0.3106)$ $ H-10 \rightarrow L+1\rangle-c.c.(0.2118)$
$X_{x\&y}$	30^1B_{1g}	4.98	$ H-1 \rightarrow H; H-8 \rightarrow L\rangle-c.c.(0.2416)$ $ H \rightarrow L+1; H-2 \rightarrow L+2\rangle c.c.(0.1882)$
	32^1A_g	4.98	$ H-7 \rightarrow L+7\rangle(0.4544)$ $ H-13 \rightarrow L+2\rangle-c.c.(0.3240)$
XI_y	37^1A_g	5.19	$ H-3 \rightarrow L+3\rangle(0.2206)$ $ H \rightarrow L+1; L \rightarrow L+7\rangle-c.c.(0.2085)$